P H Y S I C A L   R E V I E W   L E T T E R S

Parametrization of Electron-Impact Ionization Cross Sections from Laser-Excited and Aligned Atoms

Kate L. Nixon and Andrew James Murray[*]

Photon Science Institute, School of Physics and Astronomy, University of Manchester, Manchester M13 9PL, United Kingdom

A set of parameters describing electron-impact ionization from laser-aligned atoms are reported, which define the "length", "width", and "direction" of the quadruple differential cross section (QDCS) as a function of target alignment $\mathbf{k}_B$ for fixed ingoing electron momentum $\mathbf{k}_0$ and outgoing momenta $\mathbf{k}_1$, $\mathbf{k}_2$. ^{24}Mg was used, with $\mathbf{k}_0$, $\mathbf{k}_1$, $\mathbf{k}_2$, and $\mathbf{k}_B$ in the same plane. The parameters are derived for a range of $\mathbf{k}_2$ angles, with $\mathbf{k}_1$ set at 30° to $\mathbf{k}_0$. The QDCS is then determined for all $\mathbf{k}_B$. The parameters are very angle sensitive, the QDCS direction varying more than 90° as the length to width ratio varied more than an order of magnitude.

$(e, 2e)$ measurements provide a comprehensive description of electron-impact single ionization of atomic and molecular targets [1]. In these experiments an incident electron of well-defined momentum $\mathbf{k}_0$ (energy E_0) collides with and ionizes a target that has ionization energy IP. Scattered and ejected electrons of momenta $\mathbf{k}_1$, $\mathbf{k}_2$ that emerge with energies E_1, E_2 are detected in coincidence, and a triple differential cross section [TDCS $(\mathbf{k}_0, \mathbf{k}_1, \mathbf{k}_2)$] is determined. Energy and momentum conservation requires $E_0 = E_1 + E_2 + IP$ and $\mathbf{k}_0 = \mathbf{k}_1 + \mathbf{k}_2 + \mathbf{k}_I$, where $\mathbf{k}_I$ is the recoil momentum of the ion. Since correlated electrons may emerge in any direction, the triple differential cross section is defined by six variables: the polar and azimuthal angles of the outgoing electrons $(\theta_1, \varphi_1, \theta_2, \varphi_2)$ with respect to $\mathbf{k}_0$, and their energies (E_1, E_2). By defining a scattering plane, this number reduces to five without loss of generality. To further simplify the problem an experimental geometry is specified, the most common being a coplanar geometry where $\mathbf{k}_0$, $\mathbf{k}_1$, $\mathbf{k}_2$ lie in the same plane. Other geometries have also been used through to the perpendicular plane, where $\mathbf{k}_1$, $\mathbf{k}_2$ are orthogonal to $\mathbf{k}_0$ [2,3].

A substantial body of $(e, 2e)$ data has hence accumulated over time for a wide range of kinematics. The experiments have almost universally studied ionization from targets in the *ground state*, since these are relatively easy to prepare as an atomic beam effusing from a gas jet or oven. Thermally prepared ground-state atomic targets are spherically symmetric, and so the target has no preferred direction in space prior to ionization, when averaged over time.

By contrast, the experiments discussed here study ionization from ^{24}Mg atoms excited to the 3^1P_1 state using resonant, linearly polarized continuous wave (cw) laser radiation with energy $E^{3^1P_1} \simeq 4.34$ eV. This target was used since it is the lightest alkali earth easily produced as a beam. ^{24}Mg has no hyperfine structure, which is important since the laser-excited 3^1P_1 state can be fully aligned prior to the collision, the target alignment $\mathbf{k}_B$ then pointing along the linear polarization vector ε of the laser. Since the ionization cross section now also depends on $\mathbf{k}_B$, a higher-order quadruple differential cross section [QDCS $(\mathbf{k}_0, \mathbf{k}_B, \mathbf{k}_1, \mathbf{k}_2)$] is required to fully describe the kinematics of the interaction, with IP taken from the excited state $(IP^{3^1P_1} \simeq 3.30$ eV$)$ [4]. The quadruple differential cross section now also depends upon the polar and azimuthal angles (θ_B, φ_B) of $\mathbf{k}_B$ with respect to $\mathbf{k}_0$, and so seven variables are needed to describe ionization from an aligned atom. In the data presented here, the polar angle is defined as $\theta_B = \varepsilon_B$, whereas $\varphi_B = 0$.

Several theories have been developed to describe these collisions, including time-dependent and time-independent close coupling methods [5,6], R-matrix techniques [7], and distorted wave Born approximations [8,9]. The most sophisticated models include distortions in the wave functions describing incident and outgoing electrons, the target and the resulting ion, and include exchange processes, polarization of the target and ion, and postcollisional interactions. Close coupling and R-matrix methods prove accurate over a wide range of kinematics for many species (particularly light atoms); however, they are computationally intensive. Born approximations are accurate at higher energies and are faster computationally. Only Born methods have so far attempted to describe ionization from polyatomic targets, with the comparisons to experiment so far finding mixed success [10,11].

No models have yet been published that describe ionization from laser-excited targets, although several groups are working towards this goal. Since the QDCS depends upon *seven* independent variables, it is advantageous to reduce this complexity by considering methods that parametrize the cross section. To facilitate this, a new set of parameters is defined here that describe the QDCS as $\mathbf{k}_B$ is varied, while holding $\mathbf{k}_0$, $\mathbf{k}_1$, and $\mathbf{k}_2$ fixed (effectively taking a "slice" through the multicoordinate space defining the QDCS, along these fixed momentum coordinates). These

anisotropy Q-parameters can then be used to calculate the cross section as other variables change. Since the Q-parameters define the QDCS in a given geometry, their derivation provides additional information to test emerging models.

A coplanar asymmetric geometry was chosen, as in Fig. 1. The incident electrons were emitted from a gun. Mg was produced in an oven heated to ~ 800 K. The atomic beam was quasicollimated by output apertures to produce a beam with an angular spread $\sim 3°$ and diameter of 3 mm at the interaction region. The atomic beam was condensed onto a liquid nitrogen cold trap, reducing the vacuum pressure to $\sim 2.5 \times 10^{-7}$ torr with the oven operating. A gas jet was also directed at the interaction region so that helium could be used to calibrate the electron energy. A Faraday cup monitored the beam current, and collected unscattered electrons.

Two momentum analyzers detected electrons that scattered from the interaction region. Analyzer 1 was fixed at $\theta_1 = 30°$, and detected electrons with $E_1 = 20$ eV. Analyzer 2 could rotate from $\theta_2 = 35°$ to $85°$, and also detected electrons with $E_2 = 20$ eV. The analyzers are attached to turntables that rotate independently, their angles being recorded at $5°$ intervals using optocoupled encoders. Figure 1 shows the inaccessible regions, where the analyzers would either collide with other components, or be contaminated by the atomic beam.

The laser beam was directed vertically upwards into the vacuum chamber through a fused-silica window. The beam was produced by a Spectra-Physics Matisse DX dye laser, in combination with a Wavetrain doubler. The radiation was resonant with the atomic beam at a frequency of 1 050 810 723 MHz ($\lambda_{\text{vac}} = 285.296\,344\,6$ nm), as determined by a High Finesse WSU wavemeter. The laser

was actively locked to this frequency by the wavemeter, which was in-turn locked to a helium-neon laser stabilized to better than 0.1 MHz. The UV beam was directed into the chamber using three mirrors. The laser polarization angle ε was set using a BBO Glan-laser polarizer in combination with a zero-order $\lambda/2$ plate. During data collection the $\lambda/2$ plate was rotated so that the polarization direction rotated in the scattering plane from $\varepsilon = 0°$ (along $\mathbf{k}_0$) to $\varepsilon = 360°$, with coincidence data being obtained at $10°$ intervals. The laser power at the interaction region was measured as ~ 40 mW, for a beam diameter ~ 3 mm. Note that $\varepsilon_B = \varepsilon$ in these experiments.

Fluorescence from the interaction region was imaged onto a quadrant photodiode (QPD) using an internal lens. The QPD signal was monitored as a function of laser polarization, to determine the extent of radiation trapping [12]. The signal contrast was found to be better than $50:1$ as $\mathbf{k}_B$ rotated through $360°$, indicating that depolarization due to radiation trapping was negligible. Since Mg has three stable isotopes, the laser was also scanned in frequency to ensure resonance with ^{24}Mg. These scans determined that the isotope shift from ^{24}Mg to the ^{25}Mg state was 731 ± 3 MHz, and the shift to the ^{26}Mg isotope was 1408 ± 3 MHz, in good agreement with other authors [13].

Previous experiments had studied ionization from both ground $3^1 S_0$ and laser-excited $3^1 P_1$ states of Mg [4]. This provided a check of the spectrometer operation, by comparing the new results to this older data. The data presented here were taken in the same apparatus as [4]; however, a new atomic beam oven was installed in the scattering plane, and the laser beam was directed perpendicular to this plane as shown in Fig. 1. This contrasts with the experiments of [4], where the laser beam was directed in the plane opposite to the direction of $\mathbf{k}_0$, and the oven was mounted vertically. In both cases, the directions of the atomic and laser beams ensured a minimum Doppler profile when the laser was on resonance. Figure 2 shows this comparison, with the old data shifted by $+5°$. The subsequent close agreement between data sets indicates an offset occurred in the old data, most likely due to an encoding error. A careful and independent check of the scattering angles was hence carried out in the current experiments, to ensure this error did not reoccur.

The magnitude of the excited state QDCS was set relative to the ground state TDCS in [4], by measuring the relative population of excited to ground state atoms in the interaction region for $\varepsilon_B = 90°$. These results are exploited here, allowing the new QDCS data to also be normalized to the ground state TDCS. This analysis is discussed later.

Coincidence data were obtained for a set value of θ_2 with θ_1 fixed at $30°$, while ε_B varied from $\varepsilon_B = 0°$ to $360°$. Several data sets were obtained at each angle θ_2, to establish an overall uncertainty. Analyzer 2 was then moved to a new angle, and the measurements repeated. Data were
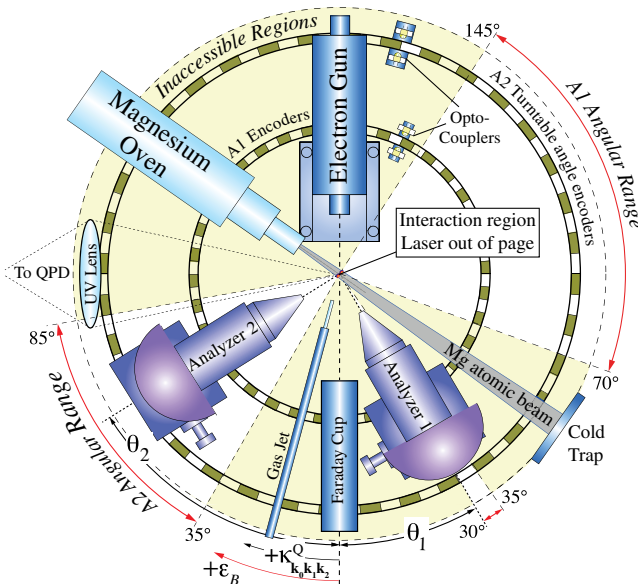

FIG. 1 (color online). The experimental apparatus, showing different components. See text for details.
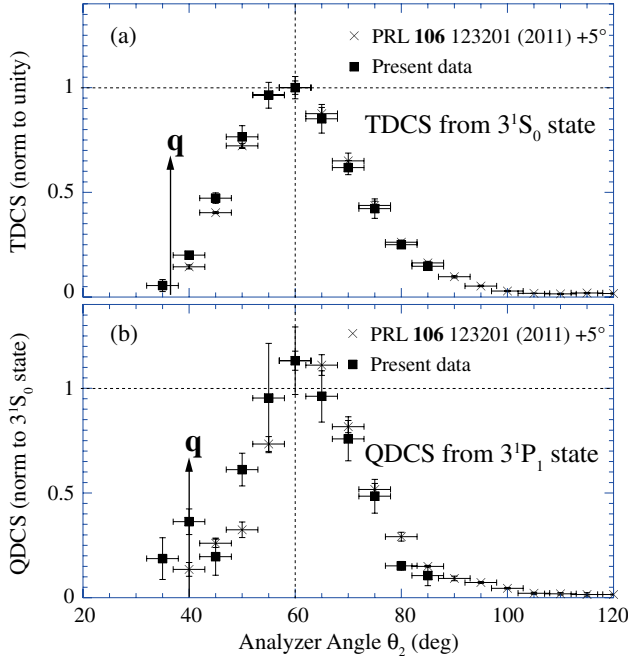
FIG. 2 (color online). Comparison of new data from (a) the ground and (b) the excited state for $\varepsilon_B = 90°$, with previous measurements [4].

FIG. 3 (color online). Polar plot of the QDCS obtained for $(\theta_1, \theta_2) = (30°, 50°)$ as a function of ε_B. A parametric fit to the data is shown. The anisotropy Q-parameter $P^Q_{\mathbf{k}_0\mathbf{k}_1\mathbf{k}_2}$ is defined by the length l^Q and width w^Q of the fit. The direction of the major axis of the fit with respect to $\mathbf{k}_0$ is given by $\kappa^Q_{\mathbf{k}_0\mathbf{k}_1\mathbf{k}_2}$. The calculated excited P-state charge cloud is shown as ε_B varies [14]. The recoil momentum direction $\mathbf{q} = \mathbf{k}_0 - \mathbf{k}_1$ is also shown.

obtained from $\theta_2 = 40°$ to $80°$, with collection times up to 2000 s for each ε_B. A full data set hence required up to 24 h to complete, during which time the laser had to remain on resonance. This exacting demand was satisfied using the active laser control described above.

An example of one of the data sets for $\theta_2 = 50°$ is shown in Fig. 3. The data display a high degree of symmetry, and are dominated by two lobes. The maximum in the cross section is offset from the incident beam and analyzer directions, and also from that of the momentum transfer $\mathbf{q} = \mathbf{k}_0 - \mathbf{k}_1$. A parametric fit to the data is shown, of the form,

$$\text{QDCS}_{\mathbf{k}_0\mathbf{k}_1\mathbf{k}_2}(\varepsilon_B) = B_{\mathbf{k}_0\mathbf{k}_1\mathbf{k}_2}(1 + P^Q_{\mathbf{k}_0\mathbf{k}_1\mathbf{k}_2}\cos[2(\varepsilon_B - \kappa^Q_{\mathbf{k}_0\mathbf{k}_1\mathbf{k}_2})]),$$

(1)

where $P^Q_{\mathbf{k}_0\mathbf{k}_1\mathbf{k}_2} = (l^Q - w^Q)/(l^Q + w^Q)$ is defined here as the *anisotropy* Q-parameter, which can vary from 0 to 1. $\kappa^Q_{\mathbf{k}_0\mathbf{k}_1\mathbf{k}_2}$ is the *direction* Q-parameter defining the angle of the QDCS maximum from $\mathbf{k}_0$. $B_{\mathbf{k}_0\mathbf{k}_1\mathbf{k}_2}$ is a scaling factor that links the QDCS at different scattering angles.

The choice of function in Eq. (1) is based upon our expectation that ionization from the 3^1P_1 ^{24}Mg state to the $3^2S_{1/2}$ ^{24}Mg$^+$ ground state will be dominated by partial waves to $L = 1$, since angular momentum must be conserved. This appears to be borne out by the data. Higher order contributions may also play a role since it is the outgoing electrons that carry this angular momentum from the interaction. It will be interesting to obtain
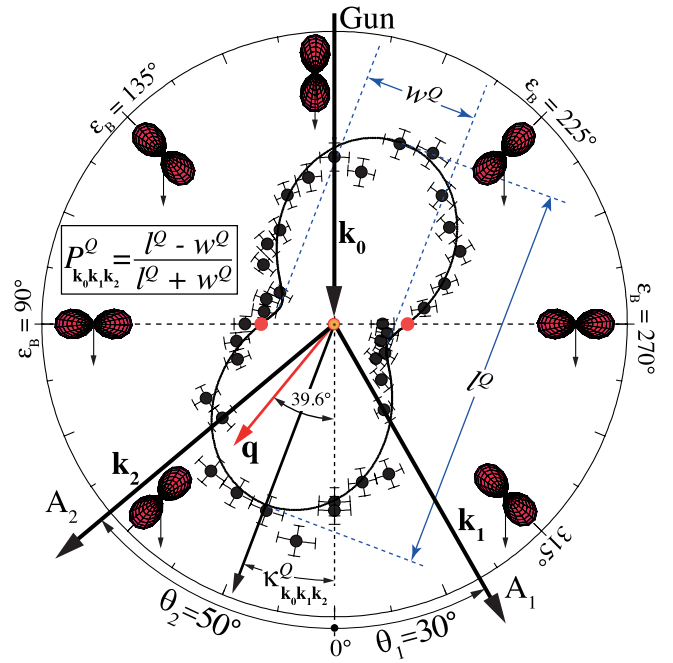
the magnitude of different partial wave contributions from future theories, to assess the accuracy of the parametric fit adopted here.

Figure 4 shows the fitted Q-parameters over the range $\theta_2 = 40°$ to $80°$. These are weighted averages from fitting Eq. (1) to several complete data sets at each angle. The angular uncertainty arises from the analyzer entrance angles (3°) and beam angle of the electron beam ($\sim 2°$). $P^Q_{\mathbf{k}_0\mathbf{k}_1\mathbf{k}_2}$ may range from 0 to 1, whereas $\kappa^Q_{\mathbf{k}_0\mathbf{k}_1\mathbf{k}_2}$ may vary from $0°$ to $180°$. The length to width ratio l^Q/w^Q is also shown, which can be derived directly from $P^Q_{\mathbf{k}_0\mathbf{k}_1\mathbf{k}_2}$.

Normalized polar plots of the fits are also depicted, demonstrating their sensitivity to both θ_2 and ε_B. $P^Q_{\mathbf{k}_0\mathbf{k}_1\mathbf{k}_2}$ is ~ 0.91 at $\theta_2 = 80°$, with a length $l^Q \sim 21$ times larger than the width w^Q. At this angle the QDCS is clearly very sensitive to the alignment direction ε_B. At $\theta_2 = 40°$, $P^Q_{\mathbf{k}_0\mathbf{k}_1\mathbf{k}_2}$ is ~ 0.66, and $l^Q/w^Q \sim 5$. By contrast, for θ_2 from $55°$ to $60°$, $P^Q_{\mathbf{k}_0\mathbf{k}_1\mathbf{k}_2}$ reduces to ~ 0.4 and $l^Q/w^Q \sim 2.3$. In this regime the cross section is more isotropic, as seen in the associated polar plots.

The direction of the fit defined by $\kappa^Q_{\mathbf{k}_0\mathbf{k}_1\mathbf{k}_2}$ changes from parallel to $\mathbf{k}_0$ at lower angles, to almost orthogonal to $\mathbf{k}_0$ when $\theta_2 \geq 60°$. $\kappa^Q_{\mathbf{k}_0\mathbf{k}_1\mathbf{k}_2}$ rapidly changes by 90° from $\theta_2 = 45°$ to $60°$, as again seen in the middle polar plots. The actual rate of change of $\kappa^Q_{\mathbf{k}_0\mathbf{k}_1\mathbf{k}_2}$ with θ_2 is greater than in Fig. 4, since the data include convolution over the spectrometer angular resolution. A Quick-time movie showing
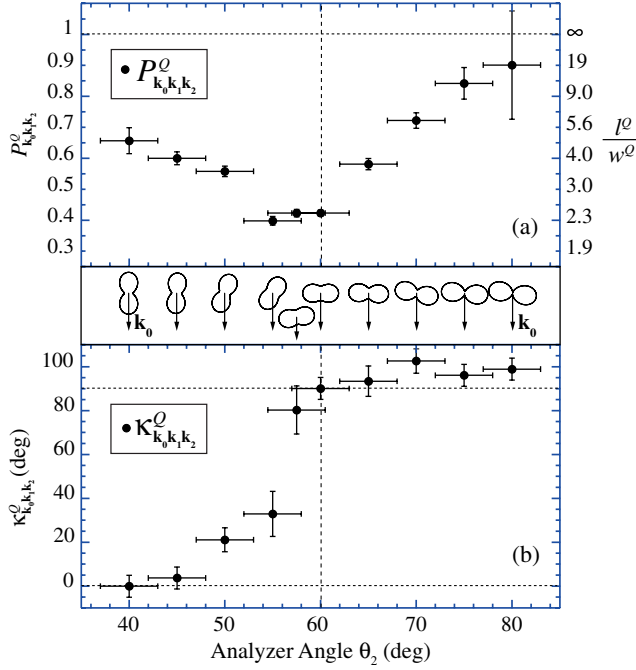
FIG. 4 (color online).   The fitted Q-parameters as a function of θ_2, defined by Eq. (1). Normalized polar plots of the fitted functions with respect to $\mathbf{k}_0$ are shown, demonstrating their rapid change in direction and shape as θ_2 varies. The ratios l^Q/w^Q equivalent to the $P^Q_{\mathbf{k}_0\mathbf{k}_1\mathbf{k}_2}$ values given on the left axis are also shown in (a) to two significant figures.

the evolution of these functions with respect to scattering angle may be viewed at [15]. These movies were generated by interpolating between the data shown in Fig. 4.

It is worth noting that under coplanar symmetric kinematics (i.e., for $E_1 = E_2$ and $\theta_1 = \theta_2$), $\kappa^Q_{\mathbf{k}_0\mathbf{k}_1\mathbf{k}_2}$ is either 0° or 90°, since the QDCS must lie parallel or perpendicular to $\mathbf{k}_0$ due to reflection symmetry in the scattering plane. The experiments described here adopted $E_1 = E_2$; however, θ_1 was fixed at 30° by apparatus constraints. Since $\kappa^Q_{\mathbf{k}_0\mathbf{k}_1\mathbf{k}_2} \sim 0°$ for $\theta_2 = 40°$, we predict that under coplanar symmetric conditions at these energies, the QDCS will orient along $\mathbf{k}_0$ for forward angles. $\kappa^Q_{\mathbf{k}_0\mathbf{k}_1\mathbf{k}_2}$ would then stay at 0° as $\theta_1 = \theta_2$ increased, unless $P^Q_{\mathbf{k}_0\mathbf{k}_1\mathbf{k}_2}$ reduced to zero at some angle $\theta_1 = \theta_2 = \theta^{(0)}$. When $P^Q_{\mathbf{k}_0\mathbf{k}_1\mathbf{k}_2} = 0$ the QDCS is independent of ε_B, and so $\kappa^Q_{\mathbf{k}_0\mathbf{k}_1\mathbf{k}_2}$ is equal to both 0° and 90°. Under these conditions $\kappa^Q_{\mathbf{k}_0\mathbf{k}_1\mathbf{k}_2}$ could then emerge at 90° as $\theta_1 = \theta_2$ increased beyond $\theta^{(0)}$. Future experiments will explore these conditions, to determine if such changes occur.

The derived Q-parameters in Fig. 4 and the data at $\varepsilon_B = 90°$ in Fig. 2(b) can be combined to determine the QDCS from $\theta_2 = 40°$ to 80°, over all possible ε_B. When $\varepsilon_B = 90°$ Eq. (1) reduces to

$$\text{QDCS}^{\varepsilon_B=90°}_{\mathbf{k}_0\mathbf{k}_1}(\theta_2) = B_{\mathbf{k}_0\mathbf{k}_1}(\theta_2)[1 - P_{\mathbf{k}_0\mathbf{k}_1}(\theta_2)\cos 2\kappa_{\mathbf{k}_0\mathbf{k}_1}(\theta_2)],$$
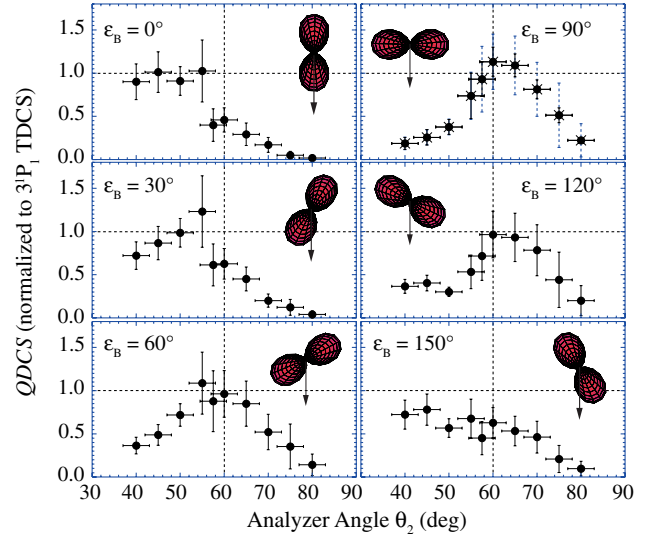
(2)

FIG. 5 (color online).   QDCS derived from the Q-parameters and data in Fig. 2(b). Examples at different ε_B are shown, normalized to the TDCS in Fig. 2(a). The data at $\varepsilon_B = 90°$ are the weighted average of the data in Fig. 2(b).

where the variation with θ_2 (i.e., $\mathbf{k}_2$) is now specified. Equation (2) effectively applies to a different region of multicoordinate space, now taken along the fixed momentum coordinates $\mathbf{k}_0$, $\mathbf{k}_1$, and $\mathbf{k}_B$. The left side of Eq. (2) is the QDCS for the 3^1P_1 state from Fig. 2(b), whereas the bracketed term on the right side may be calculated from Fig. 4. The scaling factors $B_{\mathbf{k}_0\mathbf{k}_1}(\theta_2) = B_{\mathbf{k}_0\mathbf{k}_1\mathbf{k}_2}$ can then be calculated at each θ_2. Since all factors in Eq. (1) are then determined, the normalized QDCS can be ascertained as a function of both θ_2 and ε_B.

Figure 5 shows examples of the derived QDCS as a function of θ_2, for ε_B from 0° to 150° in 30° steps. The QDCS evolves from a forward peaked structure at low ε_B through to a double peaked structure at $\varepsilon_B \sim 120°$, after which the high-angle peak diminishes and the forward peak reemerges. No obvious structure is seen at $\varepsilon_B = 150°$, the QDCS reducing monotonically as θ_2 increases over the measured range. To see the changes in detail, a quick-time movie has been generated showing the evolution as a function of ε_B. This can be viewed at [15].

The QDCS parametrization introduced here has allowed the ionization cross section for laser-excited and aligned atomic targets to be explored in far greater detail than has been achieved before. The Q-parameters presented here are for a coplanar asymmetric geometry; however, this type of analysis should be applicable to other kinematic conditions, since the structure of the QDCS must change in a symmetric way as ε_B rotates through 360°. One such analysis (the coplanar symmetric geometry) has been discussed.

The main conclusion from this work is that the ionization cross section is highly sensitive to target alignment, as

reflected in the rapid changes in both angle and shape of the QDCS observed over only a small range of scattering angles. It will be instructive to see how well theory compares to this new data, since the models are computationally challenging. It will also be instructive to see if the Q-parameters can be derived directly from theory. Such methods were proposed by Klar and Fehr [16], and were later adopted by Murray *et al.* [17] to parametrize experimental TDCS data from helium.

A detailed understanding of electron impact ionization from excited and aligned targets is important in many areas, ranging from understanding stellar atmospheres through to determining cross sections in plasmas and ion lasers. The parametrization techniques described here allow a detailed comparison to be made to new models that are currently being developed to understand these processes. Further, the sensitivity of the cross section to target alignment as demonstrated here through the Q-parameters is also likely to be important for ionization of molecules, which have inherent alignment due to their distributed nuclei. This sensitivity may explain the relatively poor agreement currently found between experiment and theory for molecular targets, since the models do not yet consider these effects in detail. The results presented here should promote further analysis of these important interactions.

*Andrew.Murray@manchester.ac.uk

[1] *Fragmentation Processes*, edited by C. T. Whelan (Cambridge University Press, Cambridge, England, 2013).
[2] M. A. Stevenson, L. Hargreaves, B. Lohmann, I. Bray, D. Fursa, K. Bartschat, and A. Kheifets, Phys. Rev. A **79**, 012709 (2009).
[3] A. J. Murray and F. H. Read, Phys. Rev. A **47**, 3724 (1993).
[4] K. L. Nixon and A. J. Murray, Phys. Rev. Lett. **106**, 123201 (2011).
[5] J. Colgan and M. S. Pindzola, Phys. Rev. A **74**, 012713 (2006).
[6] I. Bray, D. V. Fursa, A. S. Kadyrov, A. T. Stelbovics, A. S. Kheifets, and A. M. Mukhamedzhanov, Phys. Rep. **520**, 135 (2012).
[7] K. Bartschat, Comput. Phys. Commun. **114**, 168 (1998).
[8] A. Prideaux, D. H. Madison, and K. Bartschat, Phys. Rev. A **72**, 032702 (2005).
[9] M. K. Srivastava, R. K. Chauhan, and R. Srivastava, Phys. Rev. A **74**, 064701 (2006).
[10] K. L. Nixon, A. J. Murray, H. Chaluvadi, C. Ning, J. Colgan, and D. H. Madison, J. Chem. Phys. **138**, 174304 (2013).
[11] S. Xu *et al.*, J. Chem. Phys. **137**, 024301 (2012).
[12] A. T. Masters, A. J. Murray, R. Pascual, and M. C. Standage, Phys. Rev. A **53**, 3884 (1996).
[13] V. A. Korol and M. G. Kozlov, Phys. Rev. A **76**, 022103 (2007).
[14] A. J. Murray, W. MacGillivray, and M. Hussey, Phys. Rev. A **77**, 013409 (2008).
[15] es1.ph.man.ac.uk/QDCS.
[16] H. Klar and M. Fehr, Z. Phys. D **23**, 295 (1992).
[17] A. J. Murray, F. H. Read, and N. J. Bowring, J. Phys. B **30**, 387 (1997).